Fabrication and optimization of bio-silver nanoparticles: Activity evaluation against beta-lactamases-resistant *Enterococcus faecalis*

Bikhal Fattah
University of Sulaimani
Huner Arif
University of Sulaimani
Haider Mousa (haider.hamzah@univsul.edu.iq)
University of Sulaimani

Research Article

Keywords: Antibacterial resistance, Enterococcus faecalis, Silver nanoparticles, Comamonas aquatica, Fusarium solani

Posted Date: September 14th, 2021

DOI: https://doi.org/10.21203/rs.3.rs-557864/v2

Abstract

Objectives: Due to the presence of antibiotic-resistant genes, treatment options of clinical isolates are exceedingly limited. This study was aimed to fabricate, optimize, characterize, and evaluate the action of silver nanoparticles (AgNPs) against a clinical isolate of *Enterococcus faecalis*.

Materials and Methods: A combination of cell-free supernatant (C-FS) of the filamentous fungus *Fusarium solani* and Gram-negative *Comamonas aquatica* for AgNPs formation was proposed; the antigrowth and antibiofilm of AgNPs against *E. faecalis* harboring bla_{TEM} and bla_{CTX-M} genes were assessed.

Results: The ratio of 1:2 v/v (C-FS:$AgNO_3$) at pH 9.0 for 72 h in 1 mM $AgNO_3$ were the optimal conditions for AgNPs formation. UV-vis absorption peak appeared at 425 nm and the crystalline nature of synthesized particles was verified by X-ray diffraction (XRD). Fourier transform infrared spectroscopy (FTIR) analysis confirmed the interaction of protein molecules with the AgNPs. Transmission electron microscopy (TEM) analysis demonstrated that fabricated AgNPs were relatively monodispersed, approximately spherical, and of size 2-7.5 nm. bla_{TEM} and bla_{CTX-M} were detected in *E. faecalis*; the growth and biofilm of *E. faecalis* were significantly decreased by the action of 12.5 µg/ml AgNPs.

Conclusions: This is the first study proposing alternative sources to form AgNPs via synergistic metabolites of *F. solani* and *C. aquatica*. The results here offer a foundation for developing an effective therapy using AgNPs against clinical pathogens.

Introduction

In the last decade, the rate of antibiotic resistance has considerably elevated as pathogens evolve a variety of mechanisms for resistance to antibiotics (1). As a phenomenon, antibiotic resistance is often associated with infection and is therefore also related to virulence, as in the cases of biofilm-producing bacteria (2). The latter is the cause of several acute and chronic human infections such as the native valve endocarditis, pneumonia in cystic fibrosis patients, infection of chronic wounds, catheter-associated infections, and chronic bacterial prostatitis (2, 3). Most of the currently used antibiotics are becoming inefficient against the biofilm-associated and multidrug resistant (MDR) microorganisms. Therefore, it is necessary to bioprospecting for novel solutions to mitigate such microbes. (4). *Enterococcus faecalis* is one of the most common primary infectious enterococcal species identified in hospital-acquired infections (5). *E. faecalis* is a Gram-positive bacterium and is ranking among the most common nosocomial pathogens isolated from the bloodstream, surgical sites, and urinary tract infections (6). It is also involved in clinical pathogenesis such as wound infections, infective endocarditis, meningitis, and endodontic infections (7). *E. faecalis* has the ability to produce a biofilm composed mainly of specific cell surface protein (Esp), where the film plays a vital role in the adherence mechanism to surfaces, especially of medical devices in chronicle infected patients (8).

Silver nanoparticles (AgNPs) are an alternative to combating bacterial biofilms. AgNPs possess efficient antimicrobial and anticancer activities (9). Also, they are used in wound repair (10) and the promotion of bone healing (11). Silver shows less toxicity towards humans at lower concentrations; thus, it has been widely incorporated in drugs under various forms such as salts, immobilized ions, or nanoparticles (12). The exact mechanism of AgNPs against pathogens is still not clear; however, there are various proposed mechanisms of action including disturbance of the cell membrane, alteration of cellular DNA and proteins, respiratory chain blockage, or the generation of reactive oxygen species (13). Fabrication of stable AgNPs is a very challenging task; physical methods have low yields, while the chemical ones cause harmful effects on the environment due to use of toxic solvents and the regeneration of hazardous byproducts which can limit the use of AgNPs for clinical applications (14). Biogenic methods for the synthesis of NPs are a strong alternative (15). Qurbani and Hamzah (16) found that the filamentous fungus *Fusarium solani* and Gram-negative *Comamonas aquatica* grow well in co-culture and tolerate high concentrations of metals; the study reveals synergistic relationships between *F. solani* and *C. aquatica* that robustly remove metals in the culture medium (16). Here, we examined how the supernatants of *F. solani* and *C. aquatica*, cooperatively, can be used to synthesize AgNPs *in vitro*. The effect of AgNPs against a common clinical isolate of infection-derived *E. faecalis* was also studied.

Materials And Methods

Source of microorganisms

F. solani and *C. aquatica* were used as a source for nanoparticles synthesis. Both organisms were previously isolated and identified by Qurbani and Hamzah (16). For the antibacterial experiment, *E. faecalis* was selected as a model. *E. faecalis* is a clinical bacterium isolated from a urine sample in Sulaymaniyah Teaching Hospital. *E. faecalis* was identified via VITEK2 (BioMerieux, USA) instrument using a Gram-positive VITEK2 ID card.

Preparation and optimization of bio-AgNPs

Fresh cultures of *F. solani* and *C. aquatica* were grown separately in 250 ml Erlenmeyer flasks containing 100 ml of nutrient broth. The flasks were incubated at 30 °C for 48 (for the bacterium) and 72 h (for the fungus). C-FS from the culture flasks were collected by centrifugation (Biofuge Stratos, Germany) at 5,000 × g for 20 min at 4 °C. For AgNPs fabrication, an equal amount of C-FS of both organisms were mixed with 1 mM of filter-sterilized $AgNO_3$ solution (Sigma, USA, purity 99.9%) as a final concentration. The flask was kept for 72 h at room temperature under static conditions. AgNPs were collected at 14,000 × g for 20 min at 4 °C (Mikro 200R, UK) and were washed three times with sterile distilled water. The obtained precipitate was kept in a Petri dish and left in the oven for drying at 40 °C for 24 h (WT`C Binder, Germany). The dried AgNPs were scraped out and obtained in powder form for further study (17). The effects of four variables on the product yield of AgNPs were optimized by varying one parameter at a time, including $AgNO_3$ concentration (0.5, 0.75 and 1.0 mM), pH values (5.0, 7.0, 9.0, and

11.0), reduction time (24, 48, and 72 h) and volume ratio (1:1, 1:2, 2:1 v/v C-FS:$AgNO_3$). All experiments were carried out in triplicates.

Characterization of bio-AgNPs

The bio-reduction of Ag^+ ions was monitored with UV-vis spectrum and was recorded with UV-vis spectrophotometer (Kary60, USA) at a resolution of 2 nm within a range of A_{300} to A_{800} nm. FTIR analysis was carried out in the range of 400–4,000 cm^{-1} at a resolution of 4 cm−1 (PerkinElmer 1600, USA). Crystal structure and size of the AgNPs were investigated by X-ray diffraction using an X 'Pert Pro diffractometer (Pan Analytical, Netherlands) equipped with Cu-K-α radiation (1.5406 Å), at the fixed operating voltage and current of 45 kV and 40 mA, respectively. The shape and size of the AgNPs were further determined by TEM (PHILIPS model CM120, Netherlands).

Antibacterial activity of bio-AgNPs

For the agar well diffusion assay, *E. faecalis* was grown overnight in Luria-Bertani broth (LB) at 37 °C (18). CFU/ml was adjusted to be 10^8. Then, 100 µl culture broth was spread evenly on Müeller-Hinton agar plates. Wells were made using gel puncture, and 100 µl of different concentrations of AgNPs (12.5, 25, 50, 75, and 100 µg/ml) were loaded into certain wells. Afterward, the plates were incubated at 37 °C for 24 h, then the zone of inhibition was measured (mm).

Minimum inhibitory concentration (MIC) and antibiofilm activities of AgNPs were conducted according to (19) with a few modifications. Briefly, 120 µl of bacterial culture (10^8 CFU/ml) were placed in a 96-well microtiter plate. Then, 80 µl of different concentrations of AgNPs (3, 6, 9, 12.5, 25, 50, 75, and 100 µg/ml) was added. LB broth (200 µl) was used as a negative control. The plate was then incubated for 24 h at 37 °C under gentle shaking in microplate incubator-shaker PST60 HL Plus (BOECO, Germany). The absorbance of each well was measured at 600 nm using a microtiter ELISA reader (Biotech µQuant, USA). Growth percentage was calculated based on the average and standard deviation of triplicate results. Besides, 5 µl was taken from each well and spotted onto LB agar plates. Simultaneously, 5 µl was also spotted on Congo Red Agar (CRA) plates (for the biofilm experiment). The plates were then incubated at 37 °C for 18 h.

Regarding the antibiofilm activity of AgNPs, the contents in the microtiter plate wells were discarded and washed three times with 200 µl phosphate buffer saline (PBS, pH 7.2). After drying, the remained well-attached cells were stained with crystal violet (0.1%) for 30 min. The wells were then washed 3 times with distilled water after removing the excess stain. The plate was then allowed to dry at room temperature after which 200 µl ethanol (95%) was added to the wells to solubilize the stain. Then, the wells were read at 595 nm using a microplate reader (Biotech µQuant, USA). Optical density (OD) readings were then converted to percent of inhibition (%). This experiment was performed 3 times to compare and analyze the average of each result.

Protein leakage and detection of bla_{TEM} and bla_{CTX-M} genes in E. faecalis

Protein leakage from *E. faecalis* cells was determined by the A280 assay (20) using NanoDrop 2000 (ThermoFisher, USA). Briefly, bacterial suspension with an OD of about 0.2 at 600 nm (~10^8 CFU/ml) was prepared in LB and treated with 9 µg/ml AgNPs. After overnight at 37 °C, samples were centrifuged at 14,000 × g for 5 min at 4 °C using Mikro 200R centrifuge (Hettich, UK). Afterward, the collected supernatants were subjected to protein quantification. On the other hand, total genomic DNA from untreated and treated cells was extracted using Presto™ Mini gDNA Bacteria Kit (Geneaid, Italy) following the manufacture's guidelines. PCR was performed via ThermoCycler T100TM (Bio-Rad, Singapore). The sequences of the selected primers are shown in Table 1 (20); the primers were designed to amplify partial sequences of bla_{TEM} and $bla_{CTX\text{-}M}$ genes in Gram-negative *Klebsiella pneumoniae*. PCR reaction mixture setup contained 10 µl master mix, 1 µl of forward and reverse primers each, 1 µl of DNA, and 7 µl of distilled water giving a total of 20 µl. The PCR protocol for 30 cycles was as follows: initial denaturation at 94 °C for 2 min, then 94 °C for 30 s, 55 °C for 30 s, 68 °C for another 30 s, followed by a final extension at 68 °C for 7 min. The PCR products were analyzed by electrophoresis using 1% agarose gel in TAE buffer at 90 V for about 40 min, stained with ethidium bromide, and the image was captured via MultiDoc-It™ Imaging System (UVP, USA).

Table 1. Primer sequences for detection of $bla_{CTX\text{-}M}$ and bla_{TEM}

*In the following primers, F denotes forward and R denotes reverse.

Statistical Analysis

P-values were obtained (Unpaired t-test) by using GraphPad Prism 8.0.1 software Inc, CA, USA. Statistical significance was defined when the *P*-value was less than 0.05.

Results

Optimization and characterization of bio-AgNPs

In the current study, optimal formation of AgNPs was studied to achieve, primarily, good mono-dispersity, stability, better yield, and biocompatibility of the particles at 25 °C under light conditions. Initially, the extracellular biogenic synthesis of AgNPs was confirmed through the visual color change in the reaction mixture as well as via UV–vis spectroscopy**.** The intensity of the solution, gradually, changed from pale yellow to dark brown after about 18 h of incubation. Moreover, variation in reaction conditions such as $AgNO_3$ concentrations (Fig. S1), pH values (Fig. S2), volume ratios of C-FS with $AgNO_3$ solution (Fig. S3), and reduction time (Fig. S4) directly affect the synthesis. The best conditions for AgNPs fabrication (Figure 1) were at pH 9.0 for 72 h in 1 mM of $AgNO_3$ using 1:2 v/v (C-FS:$AgNO_3$).

Figure 1. UV–visible spectrum of optimal conditions of AgNPs production. **Inset**: **A.** $AgNO_3$ solution without supernatant. **B.** C-FS. **C.** $AgNO_3$ (1 mM) in C-FS solution.

FTIR analysis was carried out to identify the interactions between the biomolecules and nanoparticles (Figure 2A). Spectrum reveals the presence of eight distinct peaks at 1056, 1409, 1462, 1597, 1643, 2987, 3086, and 3279 cm-1 in the region of 400-4000cm-1. The peaks at 3279 cm-1, 3086 cm-1, and 2987 cm-1 indicate the presence of alcohol O-Hstr, primary amine N-Hstr, and alkaline C-Hstr vibration of protein, respectively. The peaks at 1643 cm-1 and 1597 cm-1 represent the C=O carbonyl group which refers to amide of protein. The other bands lie at 1462 cm-1, 1409 cm -1, and 1056 cm-1 depict the characteristic of aliphatic and aromatic organic compounds that contain C-Nstr vibration.

The crystalline structure of the AgNPs was investigated by the XRD technique. The XRD pattern (Figure 2B) shows five characteristic peaks at 2θ values of 27.84°, 32.25°, 46.26°, 54.85° and 57.52°, which can be assigned the planes of (111), (200), (220), (311), and (222), respectively. The average estimated particle size of our sample was 16.46 nm obtained from the full width at half maximum (FWHM) of the peak corresponding to 200 planes by using the Debye-Scherrer equation.

The data obtained from TEM images show that AgNPs have mostly spherical in shape, 2-5 nm in size, and relatively monodispersed, with few agglomerated particles (Figure 2C). The particle size distribution curve shows that the range of AgNPs size is 2 to 7.5 nm with an average diameter of 4.5 nm (Figure 2D).

Figure 2. Characterization of bio-AgNPs. **A.** FTIR spectrum; the boxes indicate (O-H), (N-H) and (C-H) bands of alcohol, primary amine and alkaline, respectively. C=O indicates amide band and C-N is characteristic band of aliphatic and aromatic organic compounds. **B.** XRD pattern. **C.** TEM image. **D.** Histogram analysis of the particle size distribution.

Action of AgNPs against E. faecalis

An inhibition zone was observed against *E. faecalis* (Fig. S5). To detect the lowest concentration that completely inhibits *E. faecalis* visible growth, the MIC was determined (Figure 3A). The MIC of AgNPs against *E. faecalis* is 12.5 µg/ml (p-value < 0.0001). Additionally, AgNPs reduced the biofilm formation of *E. faecalis* by 96 %. Notably, changes in the colony and its surrounding colors on CRA in the presence of nanoparticles indicate that AgNPs have a significant role as antibiofilm against *E. faecalis* (Figure 3A inset). PCR confirmed the presence of $bla_{\text{CTX-M}}$ and bla_{TEM} in *E. faecalis*. Protein leakage was also measured in the supernatant after treating the cells with 9 µg/ml AgNPs. Protein concentration was greatly elevated (7.8 mg.ml-1) in comparison with untreated cells (4.7 mg.ml-1).

Figure 3. Action of AgNPs against *E. faecalis*. **A.** Growth and biofilm inhibition. **Inset**: Five µL was taken from each well and spotted onto the LBA plate (**a**) and CRA plate (**b**). **B.** Partial DNA bands of $bla_{\text{CTX-M}}$ and bla_{TEM} (The wells next to each gene are reactions with no DNA template).

Discussion

The current paper is the first study investigating the use of C-FS of *F. solani* and *C. aquatica* collaboratively as biocatalysts for making AgNPs, shedding light on the metabolite-metabolite

interactions between both organisms. Furthermore, the present work investigates, for the first time, the role of *C. aquatica* metabolites in AgNPs fabrication. AgNPs absorbed light at different wavelengths and were excited due to charge density at the interface between conductor and insulator; the solution developed a dark brown color within a few hours. Apparently, the combination of metabolites in our C-FS provides a synergistic effect for stabilizing AgNPs leading to the excitation of surface plasmon vibrations. To increase the yield and stability of AgNPs, pH value, reduction time, C-FS with $AgNO_3$ ratio, and $AgNO_3$ molarity were studied. Controlling pH values can be used to control certain characteristics of the nanoparticles; pH 9.0 was found to be the optimal value for the maximum absorbance at 438 nm. The bioactive metabolites of the fungal-bacterial supernatant seem to be more stable and possess higher catalytic activity at alkaline pH. In acidic pH value, AgNPs aggregation was observed. Whereas at pH 7.0, there was less synthesis of NPs (data not shown). Multiple studies reported increased nano-production at alkaline pH, corroborating our result (21-23). Longer time periods also elevate nanoparticle production (24).

Consistent with most of the literature where 1 mM of $AgNO_3$ is usually used for AgNPs synthesis, although different concentrations of silver nitrate were applied, 1 mM was found to be the best. The concentration of $AgNO_3$ is a key parameter that greatly affects the synthesis process; however, very few reports studying metal concentrations for AgNPs biogenic synthesis are available. As the concentration of $AgNO_3$ decreased to 0.75 and 0.5 mM, the production of AgNPs decreased. Ma *et al*. (23) reported that a concentration of 2.0 mM $AgNO_3$ triggered the maximum production of AgNPs, with the absorbance peak at 415 nm. Moreover, AbdelRahim *et al*. (15) found that the addition of excess metal ions created very large nanoparticles with irregular morphology.

The excreted metabolites by the fungus and bacterium have a strong affinity to bind to the AgNPs surface through free amino groups, cysteine residues, or electrostatic interaction of negatively charged carboxylate groups. Moreover, the metabolites in the C-FS were not only playing roles in the reduction and capping processes but also stabilizing AgNPs. Intriguingly, a previous article examined the importance of *C. aquatica* in reducing the toxicity of metals and stimulating the growth of *F. solani* (16). Here, we propose a coupled activity of *C. aquatica* and *F. solani* metabolite that recapitulates the reported synergistic activation for AgNPs fabrication. Consequently, more data should be necessary as it might reveal the functional principles of *C. aquatica* and *F. solani* metabolites in the synthesis process and, perhaps, shed light on the reduction mechanisms.

Confirming the exact nature of the formed AgNPs, the XRD technique was conducted. As mentioned above, the XRD pattern shows some distinct peaks at 2θ values. All the reflection planes are matched and consistent with the face-centered cubic (fcc) phase of the pure crystalline silver structure's database of the Joint Committee on Powder Diffraction Standards (JCPDS). A possible reason for the variation in the average particle size might be due to the aggregation during the drying process (24). As shown in TEM image, AgNPs with an average size ranging from 2-7.5 nm were obtained. Comparably, AgNPs with a size

ranging 6-53 nm have been synthesized from *C. acidovorans* with spherical, oval, and irregular shapes with a smooth surface (17).

With that in mind, how do AgNPs, for the first time against *E. faecalis*, perform? AgNPs inhibited the growth of *E. coli, P. aeruginosa, S. aureus*, *S. enterica*, and 7 more clinical isolates of *E. faecalis* (data not shown here). Our AgNPs, based on the MIC, are able to inhibit the growth and the biofilm of *E. faecalis* even at lowest concentrations. This might be enhancing the permeability of the cell membrane, formation of free radicals, and interaction with thiol groups, affect cellular signaling (data not shown), reduction of biofilm and DNA intensity. Several mechanisms have been proposed for the bactericidal activity of AgNPs; however, the exact mechanisms remain unclear. Most likely, smaller nanoparticles have greater antimicrobial effects (25, 26) and spherical AgNPs show a larger surface area to volume ratio (27). The combination of both these properties might present stronger bactericidal activity. One of the most accepted mechanisms is that the direct contact of AgNPs with large surface areas on a bacterial cell wall could lead to produce pits, resulting in the leakage of cellular contents and, eventually, cell death (28). In certain cases, small nanoparticles of size less than 10 nm particularly, can penetrate the cytoplasm and damage the respiratory chain enzyme thus, causing damage to proteins, reducing transcriptome and inducing cell death (29, 30). As such, the cell membrane of *E. faecalis* was disrupted by the action of AgNPs, and it was clearly supported by the resultant protein content in the supernatant. This indicates that AgNPs could increase permeability and affect membrane transport due to the serious damage of cell membrane structure. Chen *et al*. (31) reported that AgNPs not only condense DNA, but also combine and coagulate with the cytoplasm of damaged bacteria, resulting in the leakage of the cytoplasmic component.

The current study has been designed to assess the mode of action against *E. faecalis*, and the results presented here are promising and warrant further investigation. Future studies aimed at assessing and producing clinically feasible sources of AgNPs for *in vivo* studies are necessary to translate these findings into clinical use. The correlation between the production of β-lactamases and the spread of resistance among isolates of Gram-positive pathogens is very high, forming serious clinical challenges (32). *E. faecalis* has the propensity to acquire resistance determinants via horizontal gene transfer, and it has shown the frequent occurrence of antimicrobial resistance, especially to tetracycline and erythromycin (33). In this context, this is the first study to shed light on the existence of bla_{TEM} and $bla_{CTX\text{-}M}$ in a clinical isolate of *E. faecalis* using primers designed to amplify them in Gram-negative bacteria. Probeing the unusual event based on sequence changes of bla_{TEM} and $bla_{CTX\text{-}M}$ in *E. faecalis* might lead to effective prevention strategies and control horizontal nosocomial transmission of organisms.

Conclusion

In this study, the C-FS combination of *F. solani* and *C. aquatica* showed synergistic effects for AgNPs synthesis. Optimization studies confirm that pH 9.0 for 72 h in 1 mM of $AgNO_3$ using 1:2 v/v (C-FS:$AgNO_3$) were the best conditions for AgNPs formation. Moreover, the small size of AgNPs and

spherical shape suggests that they are stable particles. The different behavior of AgNPs against *E. faecalis* has been noticed. Protein leakage suggests that AgNPs might disrupt the cell wall and interfere with cellular components of *E. faecalis*. The chance of acquiring resistance genes in clinical isolates calls for an effective remedy in the control and surveillance of antibiotic resistance. Although the obtained AgNPs show promising antibacterial agents, further research is strongly recommended to investigate the safe usage of AgNPs.

Declarations

Compliance with Ethical Standards

Ethics Approval

This article does not contain any studies with human participants or animals performed by any of the authors.

Conflict of Interest

The authors declare that they have no conflict of interest.

References

1. Blair JM, Webber MA, Baylay AJ, Ogbolu DO, Piddock LJ. Molecular mechanisms of antibiotic resistance. Nat Rev Microbiol 2015; 13(1): 42-51.
2. Patel R. Biofilms and antimicrobial resistance. Clin Orthop Relat Res 2005; 437: 41-47.
3. Vestby LK, Grønseth T, Simm R, Nesse LL. Bacterial biofilm and its role in the pathogenesis of disease. Antibiotics 2020; 9(2): 59.
4. Natan M, Banin E. From Nano to Micro: using nanotechnology to combat microorganisms and their multidrug resistance. FEMS Microbiol Rev 2017; 41 (3): 302-22.
5. Dale JL, Cagnazzo J, Phan CQ, Barnes AM, Dunny GM. Multiple roles for *Enterococcus faecalis* glycosyltransferases in biofilm-associated antibiotic resistance, cell envelope integrity, and conjugative transfer. Antimicrob Agents Ch 2015; 59(7): 4094-4105.
6. Fiore E, Van Tyne D, Gilmore MS. Pathogenicity of enterococci. Microbiol Spectr 2019; 7(4): 7-4.
7. Anderson AC, Jonas D, Huber I, Karygianni L, Wölber J, Hellwig E, *et al*. *Enterococcus faecalis* from food, clinical specimens, and oral sites: prevalence of virulence factors in association with biofilm formation. Front Microbio 2016; 6: 1534.
8. Tendolkar PM, Baghdayan AS, Gilmore MS, Shankar N. Enterococcal surface protein, Esp, enhances biofilm formation by *Enterococcus faecalis*. Infect Immun 2004; 72(10): 6032-9.
9. Xu L, Wang YY, Huang J, Chen CY, Wang ZX, Xie H. Silver nanoparticles: Synthesis, medical applications and biosafety. Theranostics 2020; 10(20):8996.

10. Gunasekaran T, Nigusse T, Dhanaraju MD. Silver nanoparticles as real topical bullets for wound healing. J Am Coll Clin Wound Spec 2011; 3(4): 82-96.
11. Asgary V, Shoari A, Baghbani-Arani F, Shandiz SA, Khosravy MS, Janani A, *et al*. Green synthesis and evaluation of silver nanoparticles as adjuvant in rabies veterinary vaccine. Int J Nanomedicine 2016; 11: 3597.
12. Le Ouay B, Stellacci F. Antibacterial activity of silver nanoparticles: a surface science insight. Nano today 2015; 10(3): 339-54.
13. Singh H, Du J, Singh P, Yi TH. Extracellular synthesis of silver nanoparticles by *Pseudomonas* sp. THG-LS1. 4 and their antimicrobial application. J Pharm Anal 2018; 8(4): 258-64.
14. Zhang XF, Liu ZG, Shen W, Gurunathan S. Silver nanoparticles: synthesis, characterization, properties, applications, and therapeutic approaches. Int J Mol Sci 2016; 17(9): 1534.
15. AbdelRahim K, Mahmoud SY, Ali AM, Almaary KS, Mustafa AE, Husseiny SM. Extracellular biosynthesis of silver nanoparticles using *Rhizopus stolonifer*. Saudi J Biol Sci 2017; 24(1): 208-16.
16. Qurbani K, Hamzah H. Intimate communication between *Comamonas aquatica* and *Fusarium solani* in remediation of heavy metal-polluted environments. Arch Microbiol 2020; 202(6).
17. Rudakiya DM, Pawar K. Bactericidal potential of silver nanoparticles synthesized using cell-free extract of *Comamonas acidovorans*: in vitro and in silico approaches. 3 Biotech 2017; **7**(2): 1-2.
18. Ahmed AA, Hamzah H, Maaroof M. Analyzing formation of silver nanoparticles from the filamentous fungus *Fusarium oxysporum* and their antimicrobial activity. Turk J Biol 2018; 42(1): 54-62.
19. Hamzah HM, Salah RF, Maroof MN. *Fusarium mangiferae* as new cell factories for producing silver nanoparticles. J Microbiol Biotechnol 2018; 28(10): 1654-63.
20. Barawi S, Hamzah H, Hamasalih R, Mohammed A, Abdalrahman B, Abdalaziz S. Antibacterial mode of action of grapefruit seed extract against local isolates of beta-lactamases-resistant *Klebsiella pneumoniae* and its potential application. Intl J Agric Biol 2021; 00:000—000.
21. Birla SS, Gaikwad SC, Gade AK, Rai MK. Rapid synthesis of silver nanoparticles from *Fusarium oxysporum* by optimizing physicocultural conditions. Sci World J 2013; 2013.
22. Qian Y, Yu H, He D, Yang H, Wang W, Wan X, *et al*. Biosynthesis of silver nanoparticles by the endophytic fungus *Epicoccum nigrum* and their activity against pathogenic fungi. Bioproc Biosyst Eng 2013; ***36***(11): 1613-9.
23. Ma L, Su W, Liu JX, Zeng XX, Huang Z, Li W, *et al*. Optimization for extracellular biosynthesis of silver nanoparticles by *Penicillium aculeatum* Su1 and their antimicrobial activity and cytotoxic effect compared with silver ions. Mater Sci Eng C 2017; 77: 963-71.
24. Velusamy P, Kumar GV, Jeyanthi V, Das J, Pachaiappan R. Bio-inspired green nanoparticles: synthesis, mechanism, and antibacterial application. Toxicol Res 2016; 32(2): 95-102.
25. Rodríguez-Serrano C, Guzmán-Moreno J, Ángeles-Chávez C, Rodríguez-González V, Ortega-Sigala JJ, Ramírez-Santoyo RM, *et al*. Biosynthesis of silver nanoparticles by *Fusarium scirpi* and its potential

as antimicrobial agent against uropathogenic *Escherichia coli* biofilms. PLoS One 2020; 15(3): e0230275.

26. Lu Z, Rong K, Li J, Yang H, Chen R. Size-dependent antibacterial activities of silver nanoparticles against oral anaerobic pathogenic bacteria. J Mater Sci Mater Med 2013; 24(6): 1465-71.
27. Hong X, Wen J, Xiong X, Hu Y. Shape effect on the antibacterial activity of silver nanoparticles synthesized via a microwave-assisted method. Environ Sci Pollut Res 2016; 23(5): 4489-97.
28. Barros CH, Fulaz S, Stanisic D, Tasic L. Biogenic nanosilver against multidrug-resistant bacteria (MDRB). J Antibiot Res 2018; 7(3): 69.
29. Gurunathan S, Jeong JK, Han JW, Zhang XF, Park JH, Kim JH. Multidimensional effects of biologically synthesized silver nanoparticles in *Helicobacter pylori*, *Helicobacter felis*, and human lung (L132) and lung carcinoma A549 cells. Nanoscale Res Lett 2015; 10(1): 1-7.
30. Agnihotri S, Mukherji S, Mukherji S. Size-controlled silver nanoparticles synthesized over the range 5–100 nm using the same protocol and their antibacterial efficacy. RSC Adv 2014; 4(8): 3974-83.
31. Chen M, Yang Z, Wu H, Pan X, Xie X, Wu C. Antimicrobial activity and the mechanism of silver nanoparticle thermosensitive gel. Int J Nanomedicine 2011; 6: 2873.
32. Jubeh B, Breijyeh Z, Karaman R. Resistance of gram-positive bacteria to current antibacterial agents and overcoming approaches. Molecules 2020; 25(12): 2888.
33. Woźniak-Biel A, Bugla-Płoskońska G, Burdzy J, Korzekwa K, Ploch S, Wieliczko A. Antimicrobial resistance and biofilm formation in *Enterococcus* spp. isolated from humans and turkeys in Poland. Microb Drug Resist 2019; 25(2): 277-86.

Tables

Table 1 Primer sequences for detection of bla_{CTX} and bla_{TEM}

Primer name	Primer sequence (5’-3’)	Amplicon size (~ bp)	Antibiotic resistant
blaTEM_F	GATCCTTGAGAGTTTTCGCC	530	Ampicillin
blaTEM_R	GCAGAAGTGGTCCTGCAACT		
blaCTX_F	AGACTGGGTGTGGCATTGAT	600	Cefotaxime
blaCTX_R	CCAGGAAGCAGGCAGTCC		

*In the following primers, F denotes forward and R denotes reverse.

Figures

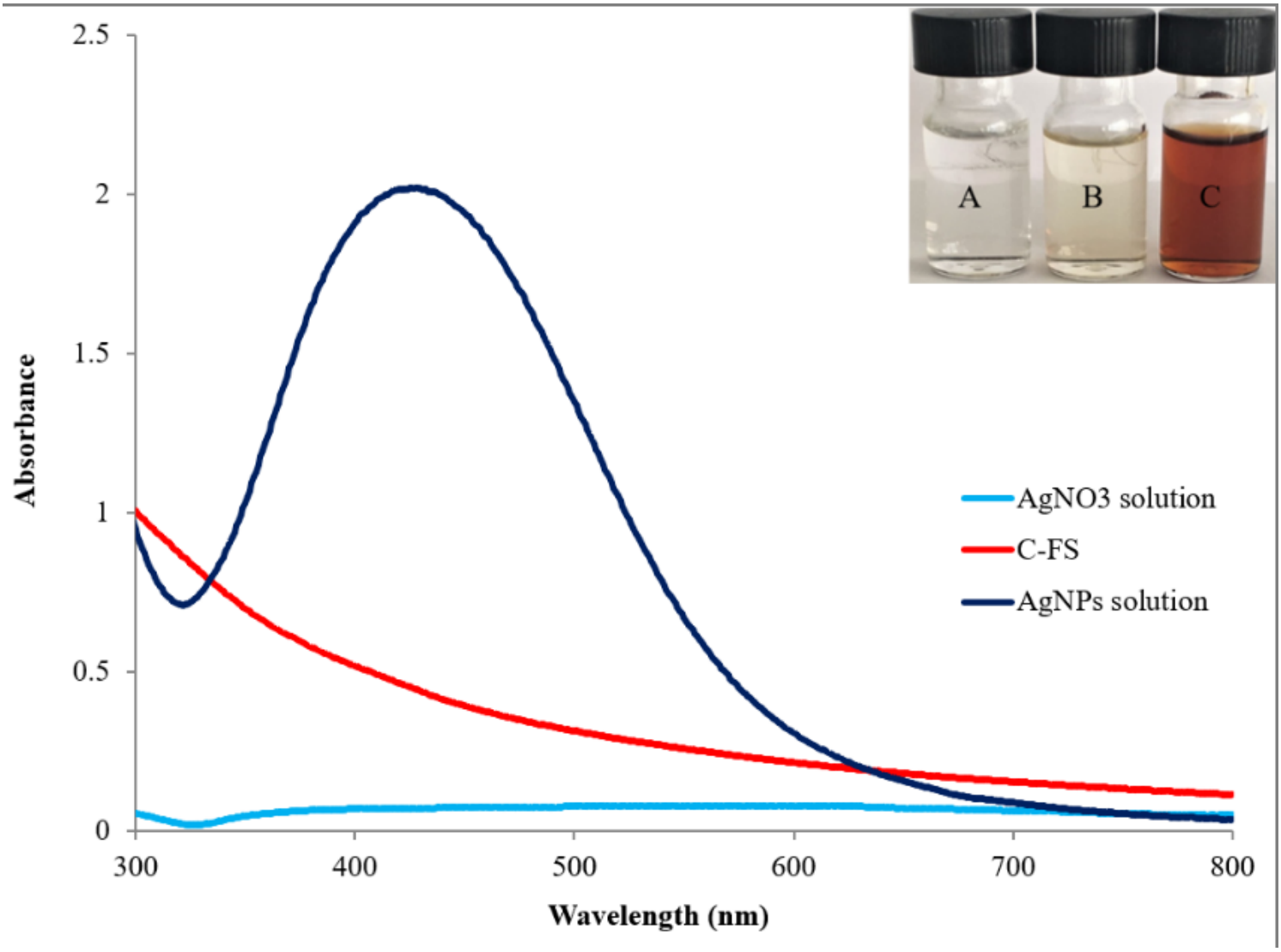

Figure 1

UV–visible spectrum of optimal conditions of AgNPs production. Inset: A. AgNO3 solution without supernatant. B. C-FS. C. AgNO3 (1 mM) in C-FS solution.

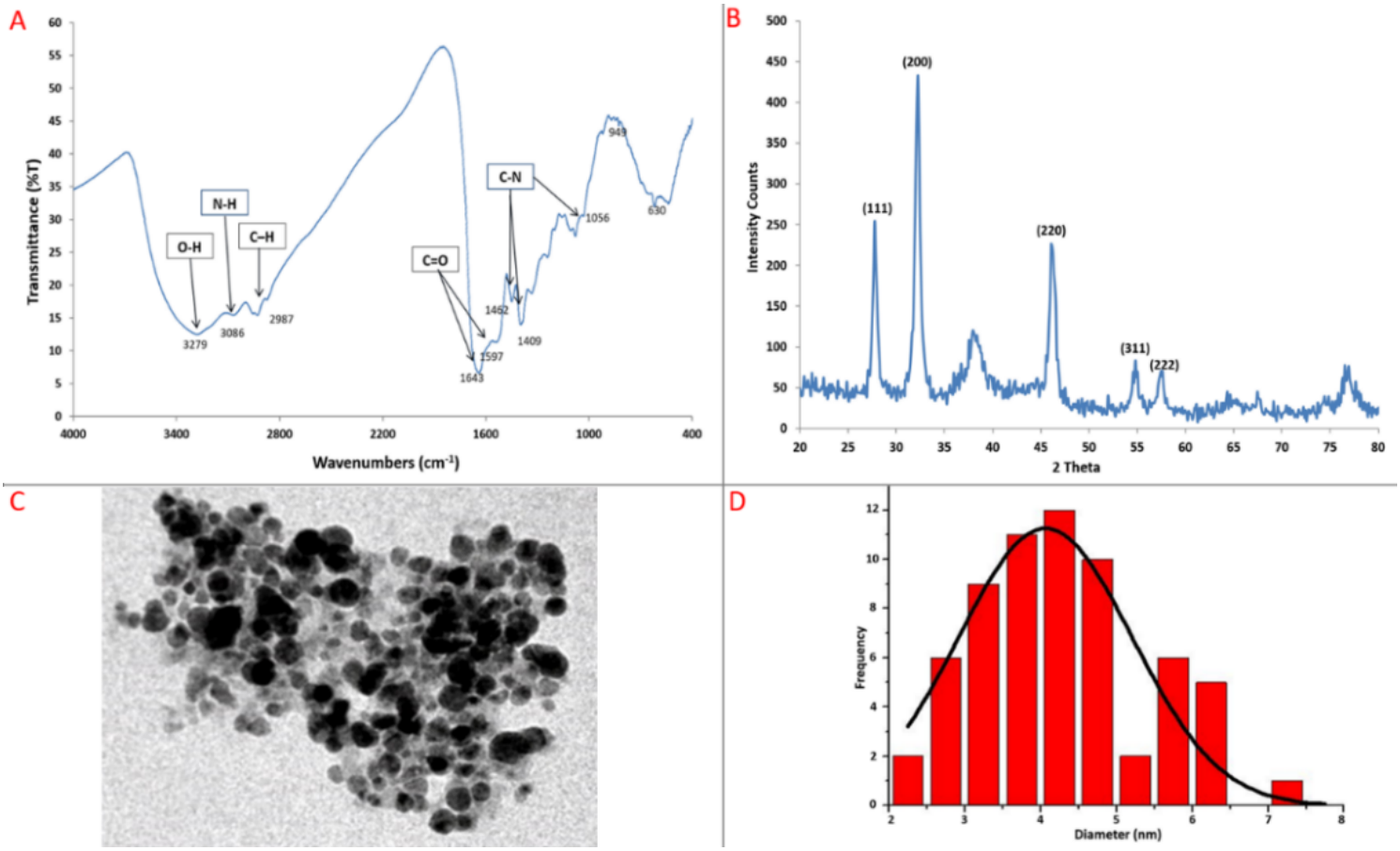

Figure 2

Characterization of bio-AgNPs. A. FTIR spectrum; the boxes indicate (O-H), (N-H) and (C-H) bands of alcohol, primary amine and alkaline, respectively. C=O indicates amide band and C-N is characteristic band of aliphatic and aromatic organic compounds. B. XRD pattern. C. TEM image. D. Histogram analysis of the particle size distribution.

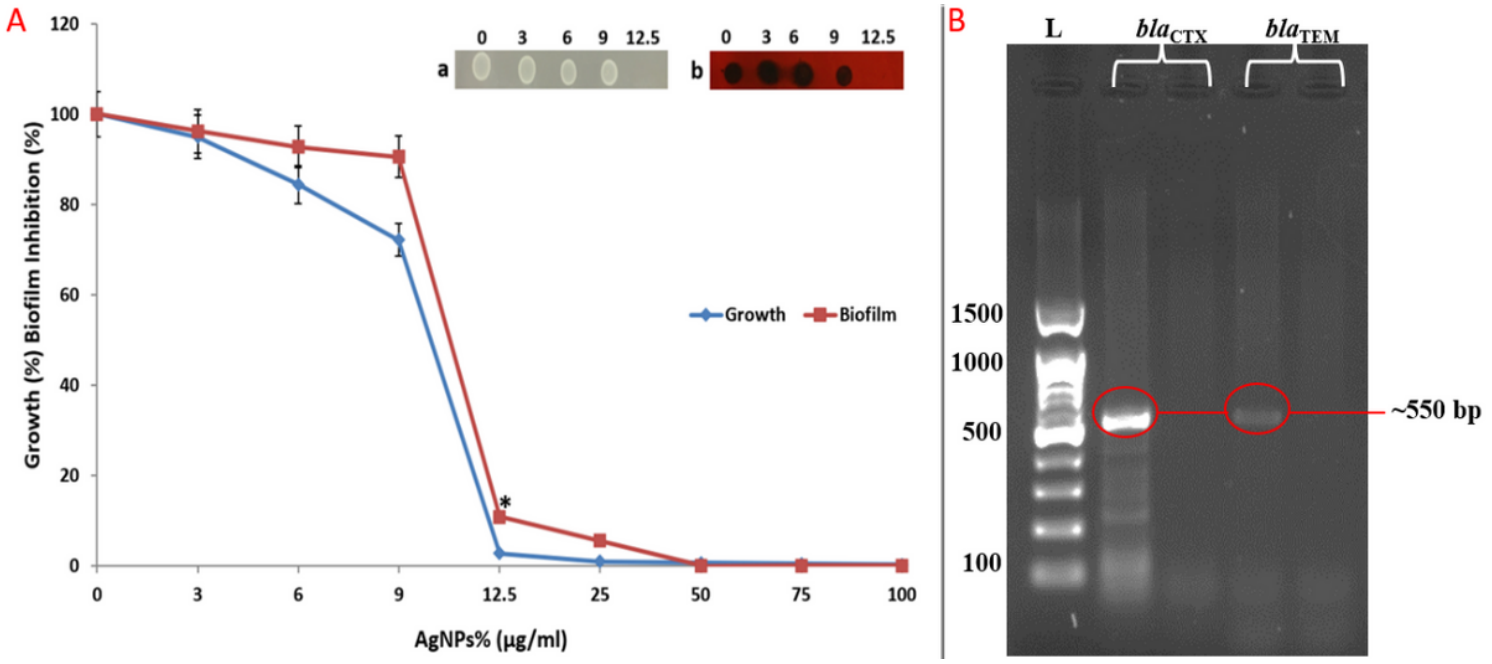

Figure 3

Action of AgNPs against E. faecalis. A. Growth and biofilm inhibition. Inset: Five µL was taken from each well and spotted onto the LBA plate (a) and CRA plate (b). B. Partial DNA bands of blaCTX-M and blaTEM (The wells next to each gene are reactions with no DNA template).

Supplementary Files

This is a list of supplementary files associated with this preprint. Click to download.

- FigureS1.png
- FigureS2.png
- FigureS3.png
- FigureS4.png
- FigureS5.png